OPTIMAL DESIGN OF AN AUTONOMOUS UNDERWATER VEHICLE

by

Shari Hannapel
Bjoern Ritter
Nick Stowe
Jeff Walls

ME 555-10-02
Winter 2010 Final Report

Abstract

Autonomous Underwater Vehicles (AUVs) play an important role in the marine industry. They are used for ship inspections, exploration of shipwrecks, and other surveying tasks. The purpose of this study was to optimize the design of an AUV used for underwater surveying by dividing the design into four subsystems: maneuvering, controls, propulsion, and vibrations.

The maneuvering characteristics of an AUV are important because mapping requires precise movement to collect high fidelity data. The maneuvering performance was optimized using an objective function which minimizes the turning radius of the vehicle. The goal of the control subsystem was to optimize a control law to achieve the desired vehicle dynamics. The objective of the propulsion subsystem was to maximize the efficiency of the propeller; this ensures that the vehicle can travel the longest distance with the least amount of power. The goal of the vibrations discipline was to minimize the amplitude of the vibrations of the hull; this ensures proper operation of any measuring apparatus which are attached inside the vehicle.

For the system integration study, the subsystem model information must be combined to form an overall system model. The system objective function was selected to be the maximization of the vehicle speed. The vehicle speed was selected to be the system objective because a faster vehicle can cover more area in less time, making an underwater survey of a specific area more time efficient. The system level problem used maximization of the vehicle speed as the objective, and each of the subsystem level objectives were converted into constraints.

Table of Contents

1. Design Problem Statement

Autonomous Underwater Vehicles (AUVs) play an important role in the marine economy. They are used for ship inspections, exploration of shipwrecks, and a myriad of other surveying tasks. AUVs have become an integral tool for oceanographic research because of their ability to operate in an environment that humans cannot easily or safely reach. Their design is a complex process requiring a balance of several performance criteria. This study discretized the design of an AUV used for general surveying applications into several subsystems including: maneuvering (Nick Stowe), controls (Jeff Walls), propulsion (Bjoern Ritter) and vibrations (Shari Hannapel). Each subsystem was then optimized for a specific objective. Finally, a global optimization for an AUV is presented.

The maneuvering characteristics of an AUV are a key component of its functionality. Mapping requires precise movement in order to collect high fidelity data. Design variables include length, diameter, center of gravity coordinates, speed and mass. The maneuvering was optimized using an objective function which minimized turning radius.

Control design for underwater vehicles is a difficult task stemming from their inherent nonlinear behavior coupled with the fact they are typically under-actuated. The success of a mission depends on the ability of a robust control law. Our goal was to optimize a control policy to dictate system inputs in order to achieve our desired vehicle dynamics. We balanced a variety of target performance criteria including control effort and ability to track a given trajectory. An accurate vehicle model served as a parameter to the study of this subsystem and was dependent upon our broader design choices such as the control surface dynamics as well as the physical dimensions of the vehicle. Through minimizing our objective function we determined the optimal control gain vector to achieve reliable and effective vehicle behavior.

The main objective of the propulsion system was to maximize the propeller efficiency. This way it can be assured that the vehicle can drive the longest distance or the highest velocity with the least amount of power. The effectiveness of the propeller was calculated using empirical data obtained from large scale model tests done by MARIN in the Netherlands.

The goal of the vibrations discipline was to minimize the amplitude of the vibrations of the hull. This helps ensure proper operation of any measuring apparatus which are attached inside the vehicle, and additionally, reducing vibration will reduce the radiated noise which may disturb sea life under observation. The amplitude of vibrations can be determined using energy finite element analysis (EFEA), with a program developed in the Naval Architecture and Marine Engineering Department. To perform the EFEA, the hull structure was modeled using a simple finite element model consisting of a cylinder, with an outer hull, longitudinal stiffeners, and transverse rings stiffeners.

For the system integration study, the subsystem model information was combined to form an overall system model. The system objective function was selected to be the maximization of the vehicle speed. The vehicle speed was selected to be the system objective because a faster vehicle can cover more area in less time, making an underwater survey of a specific area take less time. Maximization of the vehicle speed also presents an excellent overlap between the four subsystems. The system level problem used maximization of the vehicle speed as the objective, and each of the subsystem level objectives were converted into constraints. Additionally, the original constraints for each of the subsystems were included.

2. Nomenclature

2.1 Maneuvering

The maneuvering variables and parameters involve geometry, weight distributions and control fin geometry.

Objective Function Variables:

R_T - Turning Radius, meters

The design variables used are:

D - Diameter of the hull, meters

L - Length of the cylindrical section of the hull, meters

U - Forward Speed

M- Total Vessel Mass

x_{cg} - x-axis of center of gravity, meters

The design parameters are:

z_{cg} - z-axis of center of gravity, meters

f_1 - fin parameter 1

f_2 - fin parameter 2

f_3 - fin parameter 3

f_4 - fin parameter 4

f_5 - fin parameter 5

f_6 - fin parameter 6

2.2 Controls

The vehicle dynamic model was derived using methods found in Fossen (1999) and using hydrodynamic coefficients developed by Prestero (2001) for the REMUS autonomous underwater vehicle (AUV), which closely resembles our system. The following reflects the symbols and coefficients used throughout this subsystem optimization.

$\mathbf{x}(t)$	$= [\boldsymbol{\upsilon}_1^T \boldsymbol{\upsilon}_2^T \boldsymbol{\eta}_1^T \boldsymbol{\eta}_2^T \int \mathbf{e}]^T$		Vehicle state at time *t*
$\boldsymbol{\eta}_1$	$= [x\ y\ z]^T$	(m)	Earth referenced linear position vector – North, East, Down
$\boldsymbol{\eta}_2$	$= [\varphi\ \theta\ \psi]^T$	(rad)	Earth referenced angular position vector – roll, pitch, yaw(heading)
$\boldsymbol{\upsilon}_1$	$= [u\ v\ w]^T$	(m/s)	Vehicle referenced linear velocity vector – surge, sway, heave
$\boldsymbol{\upsilon}_2$	$= [p\ q\ r]^T$	(rad/s)	Vehicle referenced angular velocity vector
$\mathbf{e}$			State error, defined in Section 3.
$\mathbf{x}_f$			Final vehicle state
$\mathbf{u}(t)$	$= [H\ \delta r\ \delta s]^T$		Control signal at time *t*
H		(rad)	Commanded heading
δr		(rad)	Rudder control fin angle
δr_{max}		(rad)	Maximum rudder angle
δs		(rad)	Stern control fin angle
δs_{max}		(rad)	Maximum stern control fin angle
$\mathbf{k}$	$= [kp_p\ ki_p\ kp_h\ ki_h\ kp_z\ ki_z]^T$		Control gain vector

$J_1(\boldsymbol{\eta}_2)$		Rotation Matrix
$J_2(\boldsymbol{\eta}_2)$		Rotation Matrix
X_{udot}	(kg)	Cross flow added mass force
Y_{vdot}	(kg)	Cross flow added mass force
Z_{wdot}	(kg)	Cross flow added mass force
K_{pdot}	(kg m)	Cross flow added mass moment
M_{qdot}	(kg m)	Cross flow added mass moment
N_{rdot}	(kg m^2/rad)	Cross flow added mass moment
I_{xx}	(kg m^2)	Moment of inertia about vehicle x-axis
I_{yy}	(kg m^2)	Moment of inertia about vehicle y-axis
I_{zz}	(kg m^2)	Moment of inertia about vehicle z-axis
x_G, y_G, z_G	(m)	Position of Center of gravity relative to COB(origin)
m	(kg)	Vehicle mass
W	(N)	Vehicle weight = m/g
τ_{prop}	(N)	Magnitude of constant propeller thrust
ρ_{water}	(kg m^3)	Density of Water
$c_{L\alpha}$		Fin Lift Coefficient
S_{fin}	(m^2)	Fin Planform Area
$x_{fin}, y_{fin}, z_{fin}$	(m)	Position of fins wrt origin
L	(m)	Vehicle length
D	(m)	Vehicle hull diameter
Q,**R**		Performance index weighting matrices

2.3 Propulsion

The design variables used for this analysis are:

Variable	Unit	
A_e/A_0	1	Expanded area ratio; describes size of blades
N_b	1	Number of propeller blades
D_p	m	Propeller diameter
P/D_p	1	Pitch diameter ratio; describes the mean pitch of a blade
U_{prop}	min^{-1}	Propeller revolutions per minute

V_k	m/s	Speed of the vehicle

The parameters used for this analysis are:

Parameter	Unit	
C_d	1	Drag coefficient of AUV
D	m	Diameter of the parallel midbody
L	m	Parallel midbody hull lenght
w	1	Wake fraction (indicated fluid velocity in propeller wake field)
ρ_w	kg/m^3	Mass density of water

2.4 Vibrations

The hull of the vehicle consists of a cylindrical main body with a hemispherical nose. The cylindrical body which has six longitudinal stiffeners and ten transverse rings. Note that although the length and diameter of the hull are considered to be design variables for the global design of the vehicle, they are treated as parameters in this analysis; the nominal values used for the parameters are a length of 2 m and a diameter of 20 cm.

The objective function is the amplitude of vibration *A* (in m).

The design variables used for this analysis are (all in mm):

t_l = longitudinal stiffener thickness

t_r = ring thickness

t_h = outer hull shell thickness

t_n = nose shell thickness

t_e = end shell thickness

The parameters used for this analysis are:

D = hull diameter (m)

L = parallel midbody hull length (m)

h_r = ring height (m)

h_l = longitudinal stiffener height (m)

ρ_h = mass density of hull material (2800 kg/m^3)

ρ_w = mass density of water (1025 kg/m^3)

p = water pressure at maximum operating depth (Pa)

σ_{max} = maximum allowable stress in the hull (Pa)

3. Subsystem Analyses

3.1 Maneuvering Analysis

3.1.1 Maneuvering Mathematical Model

Objective function

The objective function, as described above, seeks to minimize turning radius while maximizing payload and length. In the beginning of the analysis, each performance point was scaled for even weighting. Therefore the objective function is defined as

$$min\ M(L, \rho_{AUV,,} R, U, x_{cg,}) = R_T + \alpha/R + \beta/L$$

Where alpha and beta are scaling factors used to normalize the terms which maximize length and payload. Even though L and R are in the denominator, it is impossible for either to go to zero, as that would indicate that the AUV had either no mass or no length. Furthermore, these variables are bounded as discussed above. Therefore there is no concern about divergence of the objective function

Constraints

The constraints on the maneuvering variables are all practical. Any conservation laws are accommodated for in the simulation model. This eliminates the necessity of physical constraints. If the model runs, the design is feasible in the Newtonian world. The constraints on dimensions are specified according to the design objectives and characteristics of similar vessels. AUV's currently used for seafloor mapping are roughly at the average of the chosen variable bounds. Hallmarks of good design were also considered. The first constraint limits the range of possible locations for the center of gravity. The bounds are chosen by assuming a somewhat even mass distribution. The center of gravity can be altered by adding weights at certain points along the length of the hull, but doing so reduces payload capacity and increases propulsive load. Thus the range was set in order to avoid a solution with center of mass at the bow or stern of the AUV.

Center of Gravity Bounds: $-0.3*L < x_{cg} < 0.3*L$

Length and diameter constraints were also set. The AUV must have a certain volume in order to carry the mapping equipment. Bounds were set based on current AUV designs with the center of the range at the average of current lengths.

Dimensional Constraints: $1.25 < L < 2.5$

$0.15 < D < 0.4$

The forward speed was bounded by a range that would require reasonable amounts of thrust. A long-range 30 mph AUV is impractical at best. Since the imaging equipment requires time to capture the topography of the sea floor, a fast vessel was not a design goal. Therefore the forward speed was bounded as follows:

$$1.0 < U < 2.0$$

The final design variable was AUV density. This is a weight per volume measurement that represents payload capacity. Based on the weight of comparable AUV's and including the desire for large batteries and extended range, the following density range was specified.

$$85 < \rho_{AUV} < 120$$

3.1.2 Maneuvering Model Analysis and Parametric Studies

The effects of variations in each variable are somewhat monotonic. In naval architecture, turning radius is quantified in terms of ship lengths. It is therefore intuitive that turning radius increases with ship length. The longer the vessel the larger pressure surface that must push water out of the way as the vessel turns. Therefore this trend is monotonic. A plot of the turning radius behavior versus ship length is shown below.

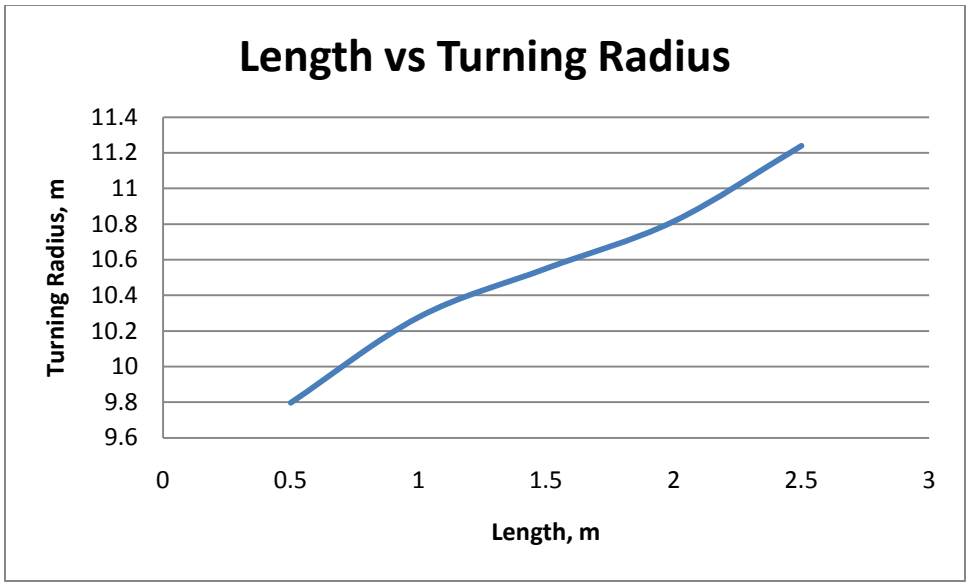

The longitudinal center of gravity has a monotonic influence on turning radius as well. Conditions for stable maneuvering are the same for ships and arrows. An arrow that flies straight has its mass located as far forward as possible. This is why the arrowhead is the heaviest part of the arrow. The second component necessary for stable flight is area located aft. This is why the feathers are at the end of the arrow. This is also why rudders are at the stern of ships. As a ship's maneuvering characteristics become more stable, it becomes harder to turn. Therefore to make a vessel turn quickest, the longitudinal center of gravity must be moved to the rear of the vessel as much as possible. This is reflected in the parametric study of x_{cg} reported below.

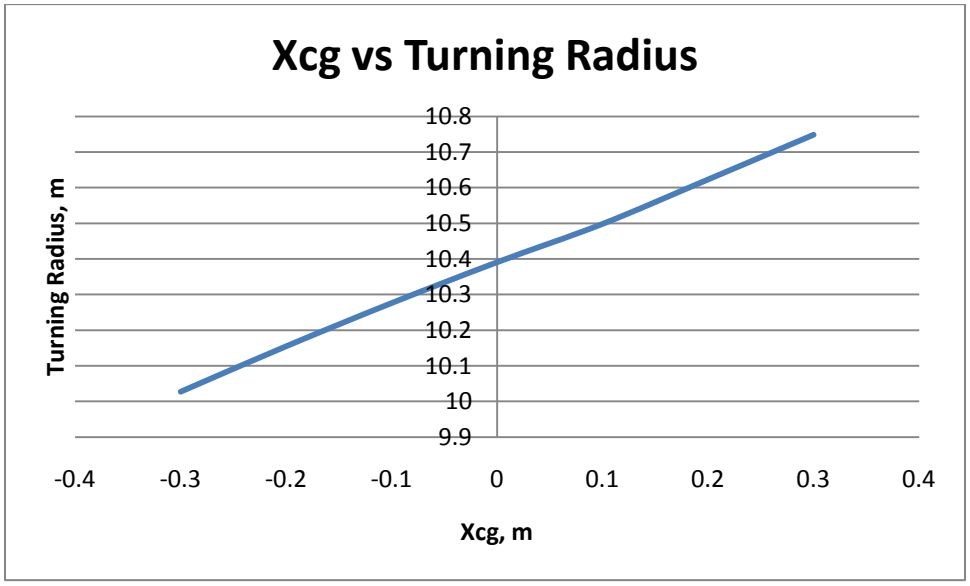

A weakness of the model is a lack of nonlinear drift terms. Under normal circumstances, the ship would drift to one side even without any rudder. Drift coefficients were calculated, but they led to the divergence of the model. Consequently they were omitted and the model fails to adequately represent the disadvantages of moving the longitudinal center to the stern.

The payload affects the turning radius, for a very simple reason: a heavier vessel has more inertia to overcome when turning, the plot below describes this relationship. Note the influence is less pronounced than other design variables.

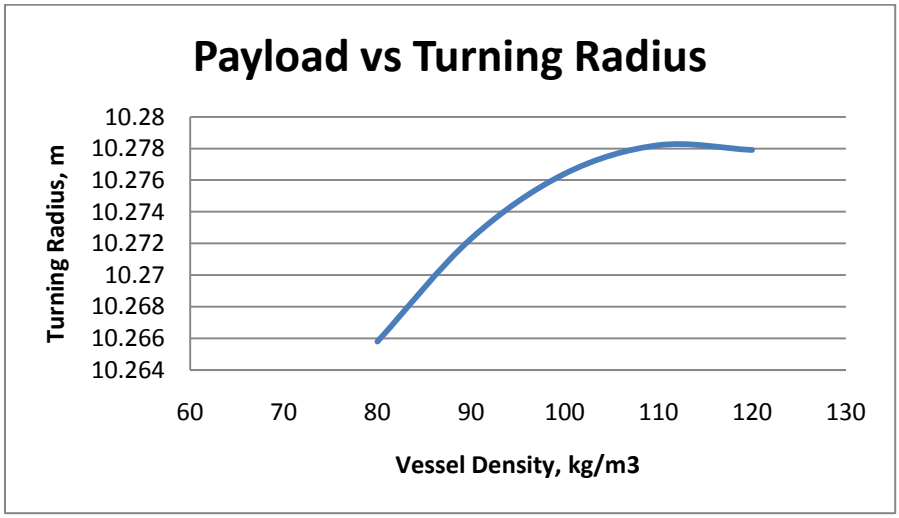

The diameter of the AUV was shown to be the most important characteristic when determining turning radius. Although its effects are monotonic, they are also highly nonlinear, as the plot below demonstrates. One would expect increasing diameter to have a similar effect as increasing length and it is very interesting that the correlation between turning radius and AUV diameter is so strong.

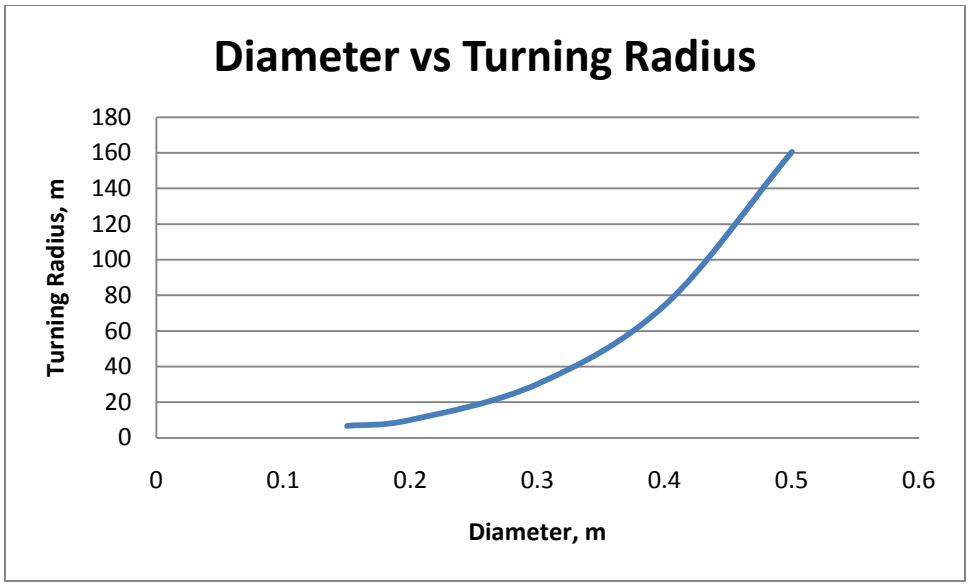

Forward speed was also shown to be monotonic. This relationship exposes a simplification of the model. A rudder works in the same fashion as an airfoil: more speed gives more lift. In the case of an AUV, this 'lift' is turning force. Therefore the turning radius should decrease with speed to a certain range, and then increase again as centripetal acceleration begins to dominate the equation. The model predicted an increasing turning radius as speed increased. this should be true for higher speeds but not for lower speeds. The problem lies in the fact that a rudder and its lift characteristics are hard to model. Turning radius versus speed plots are shown below.

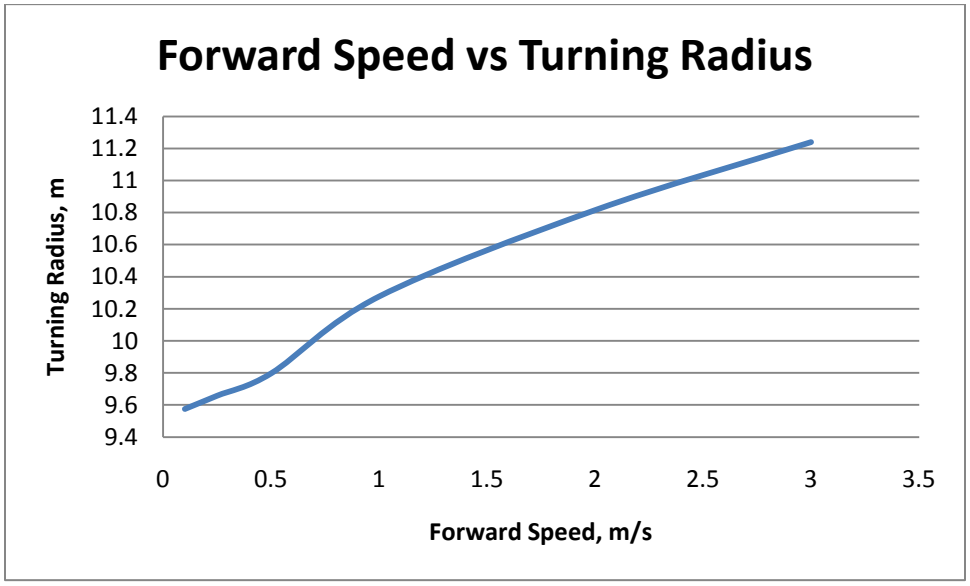

As the above discussion indicates, reaching an interesting optimum was difficult due to the monotonicity of the variables. Two of the variables are not actually monotonic; however the model oversimplifies their effects. It was not anticipated that all variables would prove monotonic. In order to make the model more interesting, payload and volumetric capacity were added to the objective function. They are each multiplied by scaling coefficients that allow the user to manipulate the importance of each design variable. If turning radius is most important, the scaling coefficients are reduced. If payload is most important, its scaling factor is increased. This approach has brought the optimum away from the variable bounds and thus yields more interesting results.

3.1.3 Maneuvering Study and Results

As previously discussed, the two dimensional maneuvering trajectory of the AUV was simulated by numerically integrating the governing differential equations that describe the motion of the vehicle. This process requires an initial velocity and rudder angle. For a given time step, the simulation code will evaluate the differential equations by using the velocity and forcing information at the current time step as initial conditions for the following time step. The maneuvering coefficients were determined using methods outlined in the Prestero thesis. The Matlab optimization tool fmincon was used to analyze the model. The variable bounds were entered using the nonlcoln nonlinear constraint input. The first analysis optimized turning radius alone and the results are predictable. The table below lists the different starting points and the resulting optimal turning radius.

Run	U	L	D	ρ_{AUV}	Xcg	Radius
1	1.25	1.5	0.3	85	-0.2	5.9240
2	1	2.5	0.2	105	0.3	5.9220
3	1.5	2	0.25	110	0	5.9240
4	2	1.25	0.15	120	-0.1	5.9240

The optimal points are listed below:

Run	U	L	D	ρ_{AUV}	Xcg
1	1.0	1.0	0.15	120	-0.3
2	1.0296	1.0	0.15	120	-0.3
3	1.0	1.0	0.15	120	-0.3
4	1.0	1.0	0.15	120	-0.3

As the results show, a global minimum clearly exists. The optimal point minimizes speed, minimizes length, minimizes diameter, maximizes payload and moves the longitudinal center of gravity as far astern as the variable bounds allow. The optimal point locates each variable at the bound that minimizes turning radius as discussed in the analysis above. It is interesting that payload is maximized, as the parametric study demonstrated a lighter vessel turns faster. The objective function contains no provisions for maximizing payload either, so the result is surprising. The only explanation is that the payload only slightly alters turning radius. Even so, if the influence is negligible it would be expected for optimal points with various payload points.

In the next set of analyses, turning radius, payload capacity, and volumetric capacity were scaled equally. The objective function was a sum of scaled turning radius, payload, and length values. This is why the objective function is approximately equal to three.

Run	U	L	D	ρ_{AUV}	Xcg	F
1	1.25	1.5	0.3	85	-0.2	2.9295
2	1	2.5	0.2	105	0.3	2.9048
3	1.5	2	0.25	110	0	2.9033
4	2	1.25	0.15	120	-0.1	2.9298

The optimal points are listed below:

Run	U	L	D	ρ_{AUV}	Xcg
1	1.4006	1.5216	0.15	120	-0.4565
2	1.0236	1.5679	0.15	120	-0.4704
3	1.0	1.5456	0.15	120	-0.4637
4	1.7128	1.5102	0.15	120	-0.4531

The results demonstrate that the composite objective function yields more interesting results. The optimal points are somewhat unstable. Note first that optimum diameter is at the lower bound of the variable. Given the results of the parametric study, this is expected. The forward speed varies significantly. This seems to indicate local minima, as turning radius and forward speed are strongly related. The minimum value of the objective function over the four runs occurs where forward speed is at its minimum bound, however. The length variable also comes off of its lower

bound for this objective function, though not by much. Density is constant, as before. The longitudinal center of gravity is again moved as far back as the constraint bounds allow.

In the next set of data, the length scaling factor was multiplied by 10 in order to emphasize this variable over turning radius and payload.

Run	U	L	D	ρ_{AUV}	Xcg	F
1	1.25	1.5	0.3	85	-0.2	10.7371
2	1	2.5	0.2	105	0.3	10.7371
3	1.5	2	0.25	110	0	10.7541
4	2	1.25	0.15	120	-0.1	10.7847

The optimal points are listed below:

Run	U	L	D	ρ_{AUV}	Xcg
1	1.0003	2.5	0.15	120	-0.75
2	1.0003	2.5	0.15	120	-0.75
3	1.3530	2.5	0.15	120	-0.75
4	2.0000	2.5	0.15	120	-0.75

We see that the results were uninteresting. Fluctuation of forward speed is present again, despite the correlation between speed and turning radius. This behavior demonstrates a weakness of fmincon.

In the final optimization exercise, the payload scaling factor was multiplied by 10.

Run	U	L	D	ρ_{AUV}	Xcg	F
1	1.25	1.5	0.3	85	-0.2	14.2371
2	1	2.5	0.2	105	0.3	14.2371
3	1.5	2	0.25	110	0	14.2371
4	2	1.25	0.15	120	-0.1	14.2397

The optimal points are listed below:

Run	U	L	D	ρ_{AUV}	Xcg
1	1.0002	2.5	0.15	120	-0.75
2	1.0002	2.5	0.15	120	-0.75
3	1.0003	2.4999	0.15	120	-0.75
4	1.0561	2.4999	0.15	120	-0.75

Like the runs emphasizing length before, the results are predictable. It is noteworthy that any noise in the optimal forward velocity point seems to have disappeared.

The above analysis demonstrates that although the variables demonstrate monotonic behavior, it is possible to reach an interesting optimum if multiple performance points are included in the objective function. The emphasis placed on turning radius, length, and payload is for the end user to decide. If the length is two times as important as the turning radius and payload, the optimum will be interesting and away from the variable bounds. If any of the three objectives is significantly more important than the other two, however, the optimal design is predictable and uninteresting. The monotonicity of each variable was not predicted at the commencement of this project. It is understood and has been clearly demonstrated that such behavior yields uninteresting optima that can be reached without any optimization. The interesting results, in this case, are found when the user determines the importance of each objective with respect to the others.

3.1.4 Maneuvering System Level Tradeoffs

Moving forward, the maneuvering subsystem design will be significantly influenced by the other subsystems. Forward speed was shown to effect turning radius. In the system level design process, the forward speed will be subject to the thrust provided by the propeller. The efficient operating range for the propeller may be above the low speeds shown to yield smallest turning radius. The structures subsystem will influence the maneuvering characteristics of the AUV as well. If a heavy structure is necessary, the payload will have to increase. Such circumstances will lead to a larger turning radius as well. The longitudinal center of gravity plays a key role in maneuvering. When it is moved toward the stern, the vessel turns quicker. It also becomes less stable. A less stable craft will require more rudder input to travel in a straight path. This represents a greater burden on the control logic. The tradeoffs between subsystems will lead to interesting results despite the monotonicity of the variables used to calculate turning radius performance.

3.2 Controls

3.2.1 Controls Mathematical Model

Objective Function

The goal of control design is to develop a control history that will transfer a system from some initial state to a desired final state. In our case, we wished to derive an optimal control history for an underwater vehicle to follow a given trajectory while also maintaining an awareness of limited power availability (motivating minimal control effort). More specifically, we were tasked with finding the optimal control gain vector, **k**, which dictates this behavior. This implementation allows us to develop the control for a single leg of a 'mow–the–lawn' survey pattern, and achieve a near optimal trajectory for each leg although they differ in initial and final conditions.

The objective function aims to produce control decisions minimizing deviations, **e**, from the ideal performance. As seen frequently in optimal control theory (Ogata, 1995), we used a quadratic performance index to determine an appropriate control law, given by

$$J = \frac{1}{2}\int_{t_0}^{t_f} [\mathbf{e}(t)^T \mathbf{Q}\mathbf{e}(t) + \mathbf{u}(t)^T \mathbf{R}\mathbf{u}(t)]dt \,,$$

where **Q** and **R** are positive definite Hermitian matrices which weight the importance of the tracking error during the control process, and control effort, respectively, and **e** is given by,

$$\mathbf{e}(t) = [(y_{desired} - y_{vehicle}),(H_{commanded} - \psi),(z_{desired} - z)]^T \,.$$

Throughout this study, we used

$$\mathbf{Q} = \begin{bmatrix} 3 & 0 & 0 \\ 0 & 0 & 0 \\ 0 & 0 & 3 \end{bmatrix}, \mathbf{R} = \begin{bmatrix} 1 & 0 & 0 \\ 0 & 0 & 0 \\ 0 & 0 & 1 \end{bmatrix}.$$

The ratios of **Q** and **R** and not their specific values are important to the objective function. Therefore, we weighted both perpendicular error to the path and depth error more heavily than their corresponding control efforts.

Our system utilizes linear feedback control so that

$$\mathbf{u}(t) = -\mathbf{k}\mathbf{e}(t) \quad \text{or} \quad \mathbf{u}(t) = -\begin{bmatrix} kp_p e_1 + ki_p \int e_1 dt \\ kp_h e_2 + ki_h \int e_2 dt \\ kp_z e_3 + ki_z \int e_3 dt \end{bmatrix},$$

with time-invariant control gain vector, **k**. Note that the state vector, **x**, consists of the vehicle state which defines **e** plus the integral of the error, thereby giving us integral control and zero-error steady state tracking as a function of our state vector. We also assume that this is available to us through a range of sensors on board the vehicle.

Given the expression of our performance index, *J*, we can describe our objective function as

$$\min_{\mathbf{k}} J(\mathbf{x}, \mathbf{k}, t) = \min_{\mathbf{k}} \left(\frac{1}{2} \int_{t_0}^{t_f} [\mathbf{e}(t)^T \mathbf{Q}\mathbf{e}(t) + \mathbf{u}(t)^T \mathbf{R}\mathbf{u}(t)] dt \right).$$

Constraints

Several constraints bound the region from which we could choose the optimal control gain vector. The most obvious and important constraint in this study stems from the vehicle dynamic model. This is a dynamic equality constraint rising from the nonlinear equations of motion expressed as

$$\dot{\mathbf{x}} - f(\mathbf{x}, \mathbf{u}, t) = 0 .$$

The dynamic constraint is composed of a complex set of nonlinear differential equations and is treated in great detail in both Fossen (1999) and Prestero (2001).

An additional physical constraint is that our control vector, **k**, must be non-negative. This is because for negative controller values, the system dynamics will diverge away from an equilibrium point,

$$\mathbf{k} \geq 0 .$$

We imposed several practical constraints either to satisfy actual limitations of our vehicle or to simplify the optimization problem. First, the vehicle fin angles need to be maintained below a certain angle due to system limitations,

$$|\delta s| - \delta s_{\max} \leq 0, |\delta r| - \delta r_{\max} \leq 0 ,$$

where the fin angle maximum for each fin is set to 45°.

An additional constraint which is logically necessary is that the path control loop cannot command a vehicle heading which is not within 90° of the path heading,

$$\left|H_{commanded}\right| - H_{path} - \frac{\pi}{2} \leq 0\,,$$

otherwise, the vehicle would be allowed to travel backwards.

In optimal control theory, final state error is often included in the objective function. We consider deviation from a desired final state not as a quantity to be minimized, rather an inequality constraint since we are more concerned with error along the trajectory rather than our final position.

$$\left|\mathbf{x}_f - \mathbf{x}_{fdesired}\right| - tol \leq 0\,,$$

where *tol* was taken to be 10 meters in our study. This constraint forced us to produce a trajectory terminating within an error region around a desired final state, yet stills allowing the vehicle to focus on maintained the desired path. By making this choice, we were also able to use a fixed end-time in the vehicle simulation which simplified evaluation of the integral within the objective function.

Design Variables and Parameters

The problem as stated thus far is dependent upon having the vehicle state space dynamic equations. Our control strategy must address vehicle motion within the depth plane (vertical position) and steering plane (plane parallel to the seafloor). We utilized the nonlinear state space representation with the full dynamic model discussed in the references (Fossen,1999, Prestero, 2001). Note that all constants appearing in the equations are dependent upon vehicle parameters such as diameter, length, fin area, mass, COG, and COB. These relationships were evaluated in Prestero (2001) for the REMUS AUV, and will be used in this subsystem optimization for their close proximity to our system.

As an important aside, we do not consider the actual fin actuator dynamics, but rather assume that the fins will exactly follow the commanded fin angles. This assumption appeared to hold valid throughout our study.

Finally, our design variables are the elements of the control gain vector, **k**. Since we control vehicle depth (single control loop) and steering plane motion (two control loops; path and yaw) the control gain vector is composed of 6 controller gains. Our system utilizes proportional-integral control in all three control loops. In this case, the control signal is a function of the current state error and the integral of the error. The integral term primarily accounts for steady state errors that proportional gain alone cannot compensate for as well as accelerating the system toward the set point. The integral term, however, can also produce an undesirable overshoot. Derivative control can also be used to eliminate some of this overshoot but was neglected in our system due to the added complexity.

3.2.2 Controls Optimization Study

As a result of using a numerical solver, as well as the complicated nature of the problem, a full monotonicity analysis proved impossible. Since the state error and control are time evolving functions of both the control and the state, we cannot fully predict their behavior a priori. We can, however, make certain observations. First, since the control is a linear function of the gains, a more aggressive (larger) proportional control gain will produce a more stiff system in which state error will be reduced. Whereas larger integral gains will decrease steady state error, but increase overshoot, so that we can expect these gains to remain small. We also notice that larger proportional gains correspond to greater control effort. Furthermore, because part of our performance index is seeking to minimize control effort, we can conclude that the gains are upper bounded and therefore the problem is well constrained.

The control signal inequalities were treated within the control logic function so as to allow a broader, and better, range of control histories. Due to the large initial disturbance used in the vehicle simulation, it is reasonable for these constraints to become active.

3.2.3 Controls Results

The nonlinear dynamics were solved throughout the optimization by taking advantage of the Matlab ode45 numerical solver and evaluating the state and control at a 100Hz sampling rate. The objective function was evaluated by running a simulation for a final time of 100 seconds

with initial errors in depth and perpendicular path distance of 5 meters each. In all cases, the vehicle long axis was initially set to point North (Earth x-axis). Matlab's fmincon was used to run the optimization by calling the objective and constraint functions. The optimization runs in approximately 30 minutes on an Intel Centrino 2.0GHz processor, making anywhere from 100-500 objective function calls. Table 3.2.1 presents the results of three optimization trials varying the initial gains.

Table 3.2.1. Optimization results for varying initial gains

Trial	$\mathbf{k}_0$						$\mathbf{k}_*$						J_*
1	1.0	0.01	1	0.1	3	0.10	0.190	0	1.06	0.64	6.27	0.0046	8.54349e2
2	0.5	0.01	5	0.0	5	0.01	0.192	0	1.06	0.64	6.28	0.0047	8.54347e2
3	0.2	0.50	10	0.5	10	0.50	0.192	0	1.06	0.64	6.28	0.0047	8.54347e2

Following typical control design, the initial gain vector includes relatively small integral gain terms. Figure 3.2.1 illustrates the effect of altering gain terms on the resultant trajectory in the depth plane. Notice that larger integral gains produce larger overshoots, while larger proportional gains result in a faster convergence. The results of the numerical optimization suggest that J is a convex function as each of the initial gain conditions results in a numerically similar minimum cost and gain vector.

Figure 3.2.1. Steering plane trajectory for various path control gains.

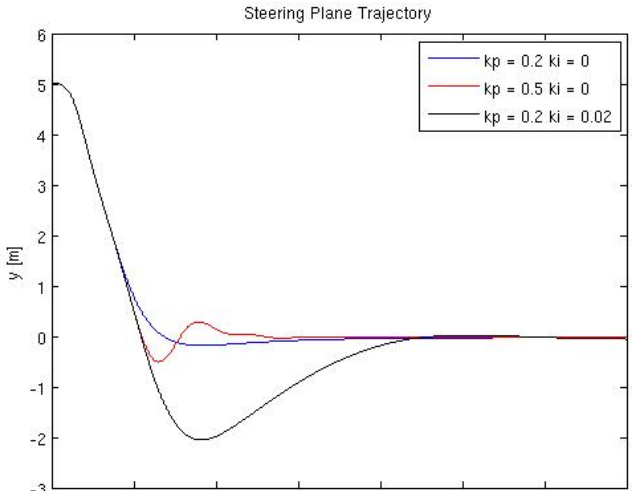

As a parametric study, we chose to observe the effect of altering subsystem parameters including fin planform area, S_{fin}, and distance between the center of buoyancy and the fin posts, x_{fin}, as these readily relate to the performance of our controller. The results of this study are presented in Tables 3.2.2 and 3.2.3.

Table 3.2.2. Optimal gain vector and cost for variation in fin planform area

Fin Area	$\mathbf{k}_*$						J_*
S_{fin}	0.192	0	1.06	0.64	6.289	0.0047	8.54347e+2
90% S_{fin}	0.2318	0.0003	5.3469	0.4540	1.1248	0.0005	9.51821e+2
110%S_{fin}	0.5115	0.0017	1.4264	0.4515	18.2753	0.0017	8.23999e+2

Table 3.2.3. Optimal gain vector and cost for variation in fin moment arm

Moment arm	$\mathbf{k}_*$						J_*
x_{fin}	0.192	0	1.06	0.64	6.289	0.0047	8.54347e+2
90% x_{fin}	2.9577	0.02559	5.7829	8.33e-7	24.7191	8.63e-5	1.06215e+3
110% x_{fin}	0.2606	0	1.1360	0.7018	6.4618	0.0050	8.60307e+2

These results are all consistent with what we would expect to see. The control effort decreases with larger fin area because less fin movement will produce an equivalent vehicle motion. Varying x_{fin} gives a less intuitive outcome, but one that can still be explained. Fin angle results in a force and a moment giving rise to motion in the opposite direction of the force. Therefore, we can expect the value of x_{fin} to balance the desired force and moment.

3.2.4 Controls System Level Tradeoffs

As can be seen from the parametric study in the previous section, the optimal control law is quite dependent upon other vehicle parameters which are being optimized as members of other subsystems. The final vehicle dimensional values dictate the dynamic model given to this control optimization. While the control design does not directly influence other areas of optimization, certain combinations of vehicle parameters can produce undesirable marginally-unstable or oscillatory behavior. An example of one such parameter is x_{fin}, which is sensitive to changes as seen in Section 5. Therefore, these particular combinations may need to be excluded from our future study of a globally optimal AUV.

Other parameters, such as the thrust delivered by the propeller, will greatly affect control performance. In the example of thrust, a greater forward speed correlates to greater control

surface forces, so we can expect increased thrust to have a similar result to increasing S_{fin}, which we saw gave an improved performance. By working with a global objective function that includes control effort and state excursion as in this study, the control optimization will indirectly influence the choice of more concrete design variables.

3.3 Propulsion Analysis

3.3.1 Propulsion Mathematical Model

Objective Function

The objective function is the efficiency of the propeller. As a numerical model is used an analytical function is not available. In general the function can be expressed as

$$\text{Max } \eta_0 = f\,(N_b,\, A_e/A_o,\, P/D_p,\, D_p,\, U,\, V_k)$$

The code generates curves for the non-dimensional thrust and torque coefficients given as

$$K_T = \frac{T_k}{\rho_w \cdot U^2 \cdot D_p^4} \text{ for thrust, and}$$

$$K_Q = \frac{Q_k}{\rho_w \cdot U^2 \cdot D_p^5} \text{ for torque.}$$

The thrust needed is calculated by the formula

$$T_k = 0.5 \cdot \rho_w \cdot C_d \cdot V_k^2 \cdot \left(\frac{D}{2}\right)^2$$

Calculation of the torque can be neglected, since the matching of the propeller will be done with the needed thrust.

The code then finds the intersection between the thrust and the K_T and interpolates from there the efficiency for the best feasible P/D_p ratio according to considerations listed below.

The advance coefficient represents the non-dimensional length the propeller “screwed” itself through the water during one turn.

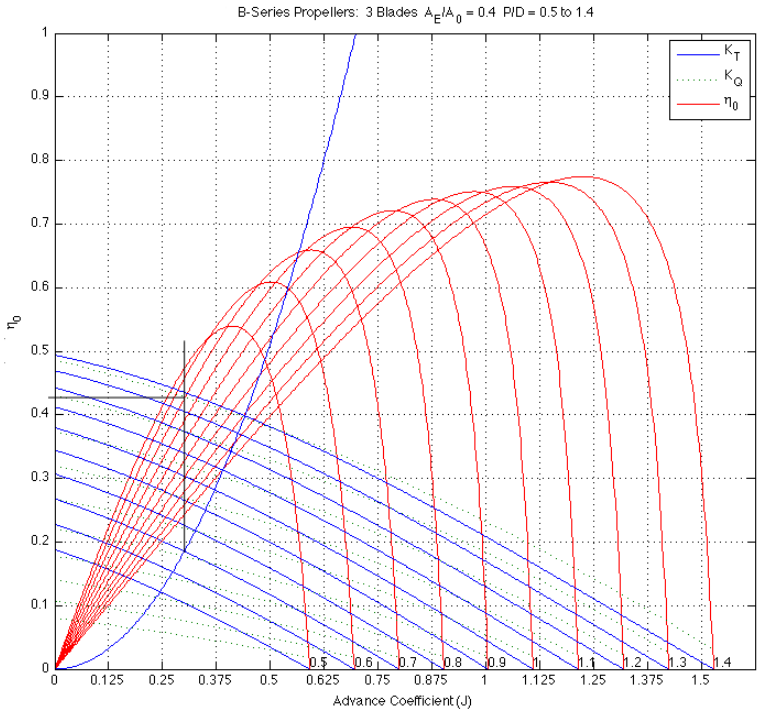

Figure 3.3.1: Example plot for eta0 = .42

To evaluate the code I compared it to the "Propeller Optimization Program (POP)" developed in the Naval Architecture and Marine Engineering department. The results have been very close. The difference encountered is fairly easy to explain since the POP uses a different method of evaluating cavitation limits than the code based on MARIN's coefficients.

Constraints

Since my propeller model is not an analytical but a numerical one no constraint functions appear. Nevertheless the design variables are bounded for different reasons.

Number of blades N_b : [2, 4]

The lower bound of two blades is quite obvious since a single bladed propeller would not be symmetric and induce very high vibrations into the system. It should be mentioned though, that according to the classical propulsion theory a single bladed propeller has the highest efficiency due to its superior ratio of wetted surface area and thrust per blade. Additionally the interference effects between multiple blades do not exist.

The upper bound has two practical reasons: Due to the given maximum diameter of the propeller, an increasing number of blades results in a decreased profile length which weakens the stability of the blade and complicates the production unreasonably. Furthermore the interference effects between the propeller blades increase. They can be reduced for one turning direction of the propeller, creating a virtually non-efficient propeller when turning in the opposite direction. Given that the AUV requires the propeller to turn backwards to stop or reverse the design with more than 4 blades becomes infeasible.

Expanded Area Ratio A_e/A_0 : [0.4, 1.05]

The Expanded Area Ratio describes the unwound propeller blade area divided by the circular area given by $A_0 = \pi * \left(\frac{D_p}{2}\right)^2$. Given that the efficiency of a propeller is the ratio of resistance and thrust, a lower Expanded Area Ratio generally leads to a higher efficiency. Nevertheless the ratio has to have a lower bound since manufacturing of very slender profile becomes pricy and the stress in every propeller blade root too high. Furthermore the pressure gradient behind very slim blades can reach a level where cavitation is likely to occur.

The upper bound is dictated mostly for manufacturing reasons, since a ratio of greater than 1 results in overlapping blades and the need for very a complicated and expensive production process. Additionally the interference between the propeller blades would decrease its overall efficiency.

Pitch Diameter Ratio P/D_p : [0.5, 1.5]

The Pitch Diameter Ratio is a non-dimensional coefficient to describe the pitch angle of the propeller blades. In terms of efficiency a high pitch is favorable because it allows for lower RPM of the propeller and therefore less friction. But since a high pitch is the major cause for cavitation a lower then theoretically ideal pitch often has to be used.

The upper and lower bounds are given by the imperial data available. They cover the most common ratios for low and fast turning propellers.

Propeller Diameter D_P : [0.33, 0.5] ft

From physical observations it is quite easy to understand that a propeller should be as big in diameter as possible. Since slowly accelerating a large quantity of water gives a better efficiency than a rapid acceleration of a smaller amount. Therefore the diameter should always be as big as possible.

Hence the lower bound is not as important as the upper bound, but has to be considered still since the propeller design must be feasible to be built.

The upper bound is restricted by the diameter of the AUV itself. The water flowing around the torpedo shaped vehicle will always be slower than the actual speed through water due to viscous frictional effects. It is then important to keep the entire propeller within this slower flowing wake field. If the tip of a blade would penetrate the wake field and reach into the faster flowing water, the resulting pressure difference for the tip of the blade would be different then for the rest of the blade. This would lead to an enormous amount of vibrations to be induced into the shaft and therefore the whole vehicle. Furthermore the maximum diameter has to be limited to limit the maximum weight of the propeller. Since a very heavy propeller in the back would unbalance the whole vehicle.

Propeller Speed U_{prop}

Following to the reasoning for the propeller diameter, a propeller should always turn as slowly as possible. But given the limitations of a high pitch to diameter ratio, mainly cavitation, a slow turning small propeller is impossible to achieve. Therefore the model will find the optimum geometry for the propeller in terms of efficiency and cavitation and then match the propeller revolutions. Since the selection of an electric motor is not part of this optimization problem the maximum revolutions per minute is unbounded and will only be determined to match the best efficiency.

Vehicle Speed V_k : [2, 3.5] ft/s

The AUV's velocity determines the thrust necessary to propel it. Given a known drag coefficient the thrust necessary is determined by the equation $T = 0.5 * C_d * \rho * V_k^2 * A$. It is obvious that the thrust increases quadratically with the velocity.

The bounds on the velocity are given by the proposed use of the vehicle. For long range operations a speed as low as feasible will be used, for quick scans of the environment a speed as high as possible.

3.3.2 Propulsion Model Analysis and Optimization Study

My model uses the DIRECT algorithm used in gclsolve.m to optimize the given values. The reason being that the number of blades has to be an integer variable, which is difficult to handle with fmincon.

The executable file calls then the optimizer and hands over 4 variables (N_b, A_e/A_0, D_p, V_k) which are bounded within the executable. The P/D_P ratio range is being divided in steps of 0.01 within the optimizer as the optimum efficiency can only be determined by matching the thrust needed with a P/D_P ratio as explained above.

The iteration is stopped after 25 iterations as no significant improvement can be achieved in additional iterations.

Well Boundedness

Since my numerical model does not have any constraints and all variables have upper and lower bounds the model can be assumed well bounded. The increasing friction that occurs at increasing relative velocity of the blade and the water limits even the unbounded variable U_{prop} describing the propeller revolutions above. The lower limit is given by the minimum thrust has to be reached. Given the limitations in geometry this results in a reasonable minimum speed for the propeller.

Constraint redundancy

Since no constraint was used and every variable is bounded up and below not constraint is likely to be redundant. Given the complexity of the model it is unfortunately not possible to check if certain geometries or speeds result in designs were bounds could be redundant.

Constraint Activity

Several constraints are active for the following reasons. The propeller diameter reaches its upper bound. Given the hydrodynamic theory behind a propeller it is obvious that a bigger slow turning propeller will always be more efficient than a smaller fast turning one. The efficiency of a large and slowly water mass has less loss due to viscous effects than a smaller one being accelerated very fast. This rule holds for every propeller design which can be seen in modern ships as well were a stern is design with the highest priority given to accommodate the biggest propeller possible.

Scaling

Since optimizers work best when the inputs are within the same order of size the variables have been scaled. While N_b has to remain an integer and is therefore limited to the range of [2, 4] it was necessary to scale some of the other variables. A_e/A_0 was multiplied by 10 to be calculated within the range of [4, 10.5], so was D_P to cover the range of [3.3, 5].

3.3.3 Propulsion Results and Parametric Study

Optimal Result

The optimum of the system described here was found to be:

Variable	Value
A_E/A_0	0.40
N_b	3
D_P	0.5 ft
P/D_P	0.74
U_{prop}	566.3 rpm
V_k	3.14 ft/s

Resulting in a efficiency η_0 = 51.9%, which is an excellent result for a propeller that small. It is not surprising that the A_E/A_0 ratio turned out to reach the lowest value possible since a shorter

profile length results in less drag while the propeller diameter reaches the upper bound due to the impulse effects described earlier.

Rather surprising is the number of blades N_b not to hit the lower bound since usually the least amount of blades results in the smallest loss. Furthermore I expected the velocity to be close to the lower bound, since the drag of the vehicle would be the lowest there. Hence it was shown that the combination of a 3 bladed propeller with the geometry shown above reaches its best performance not at the lowest speed suggested, but at the point of highest efficiency for the propeller.

Since the DIRECT algorithm I used is searching for a global minimum, it can be assumed the values above represent the global minimizer x*.

Parametric Study

Monotonicity in Propeller Diameter

To prove the often-mentioned fact that the efficiency of a propeller increases monotonically with its diameter I conducted a parametric study for D_P from diameters of .35 to .6 feet.

To be able to compare the results the number of blades was hold fixed while the rest of the geometry was allowed to change. The result shows a clearly the suspected monotonic behavior.

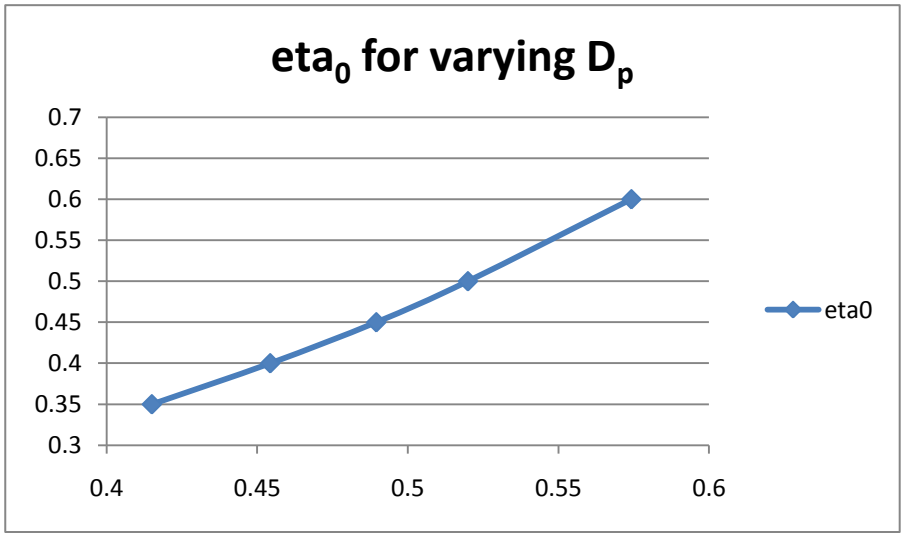

Monotonicity in Expanded Area Ratio

Contrary the efficiency should decrease with higher A_E/A_0 ratios since the profile length increases and therefore more friction occurs. To show the monotonicity the number of blades was once again held constant while the A_E/A_0 ratio was increased. The other variables could nevertheless adapt to the increasing profile length and change accordingly to limit the loss of efficiency. Nevertheless the influence of the increased expanded area ratio is clearly visible.

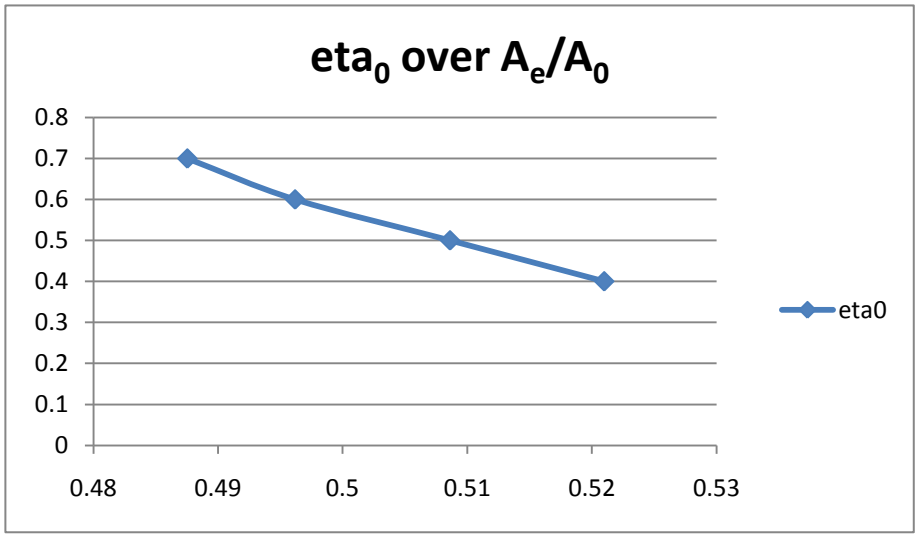

Evaluation of η_0 over speed

Since the optimal result having picked a 3 bladed design is rather surprising a parametric study shall show the differences in efficiency with more or less blades. To be able to compare the solutions obtained all parameters but the number of blades will be held constant.

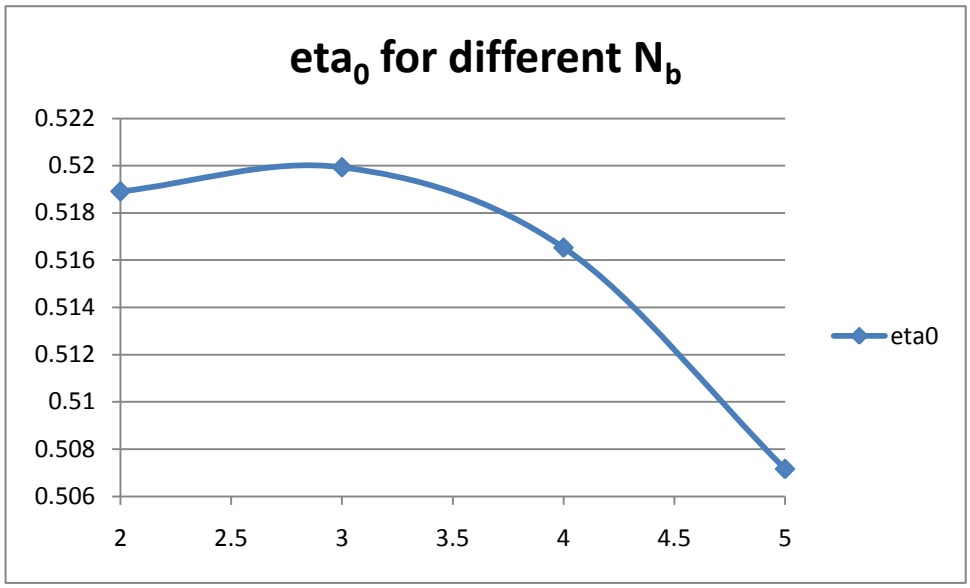

It can be seen that the differences in the efficiency for different N_b is rather small. This can be explained by the geometry of the propeller. Since only a low thrust is needed for the AUV the airfoil shape of every blade is very thin, giving a small difference in the length of the upper and lower side. Therefore having more blades increases the overall wetted propeller surface only minimal, causing very little more drag.

This explains that the best tradeoff between profile thickness and profile length is found when a 3 bladed propeller is being used.

3.3.4 Propulsion System Level Tradeoffs

Optimizing the AUV vehicle for maximum range is more than shrinking it to the smallest system possible and reducing the drag to a minimum. In order to optimize range the diameter should be as small as possible to reduce drag, contrary it should be increased to allow for a bigger and more efficient propeller. To reduce the friction along the parallel midbody it seems favorable to reduce the vehicle length, but this would lead to a more unstable vehicle for which more rudder control is necessary to keep it on the predetermined path. But an increased control effort induces more drag into the system and would therefore reduce the overall efficiency. To minimize vibration induced from the propeller a certain rpm is going to be needed. But a fixed rpm during the optimization progress could lead to a lower overall propeller efficiency. Nevertheless the

tradeoff could be acceptable if the lower vibration within the system reduce the control and steering effort.

3.4 Vibrations Analysis

3.4.1 Vibrations Mathematical Model

In this analysis, mathematical models were developed for the objective function and constraints.

Objective

The objective function to be minimized is the average vibration of the hull. The analysis was performed using an energy finite element analysis (EFEA) program developed by a professor in the Naval Architecture and Marine Engineering department. This program has been successfully applied to a number of structural design problems, including aircraft design (de Lima et al. 2009, Zhang et al. 2009) and automotive design (He et al. 2009). For small models, especially those without an acoustic analysis (as in the case with the underwater vehicle), the EFEA program runs quickly; therefore, the EFEA program was included directly in the optimization, rather than generating a metamodel from sample points.

The EFEA program was treated a "black box"-type simulation, meaning that the details of the calculations done by the program were not available to the user. However, a brief discussion of the principles of EFEA is useful, with the following summary information from (Vlahopoulos, Wu 2010). EFEA is useful for efficiently computing the vibration and acoustic response of complex structures. The governing differential equation for EFEA describes the power flow and energy flow of the system:

$$-\frac{c_g^{\,2}}{\eta\omega}\nabla^2\langle e\rangle + \eta\omega\langle e\rangle = \langle \Pi_{in}\rangle \qquad (1)$$

where $\langle e\rangle$ is the average energy density, c_g is the group velocity, η is the structural damping factor, ω is the radian frequency, and $\langle \Pi_{in}\rangle$ is the input power to the system. The governing equation is formulated in terms of averages; because the solutions vary exponentially with space, only a small number of elements is needed to describe the variation.

To solve the governing equation numerically, the following finite element formulation is used:

$$[K^e]\{e^e\} = \{P^e\} + \{Q^e\} \qquad (2)$$

where $\{e^e\}$is the vector of energy densities at the nodes of an element, $[K^e]$is the element system matrix, $\{P^e\}$ is the vector of external power input at the nodes of an element, and $\{Q^e\}$ is the vector of internal power flow across the element boundary. The superscript *e* indicates that the terms concern the element.

For the application of the EFEA program to the underwater vehicle design, the first step was to create a finite element model for the hull structure. The commercial code Hypermesh was used to create the model; Figures 3.4.1 and 3.4.2 show the meshing of the hull. Note that the finite element mesh is fairly coarse; although this mesh may not be acceptable for the determination of stresses in the structure in standard FEA, the mesh is fine enough for EFEA because this technique focuses primarily on the sizes of the plates and their connections, and not on the stresses in the structure.

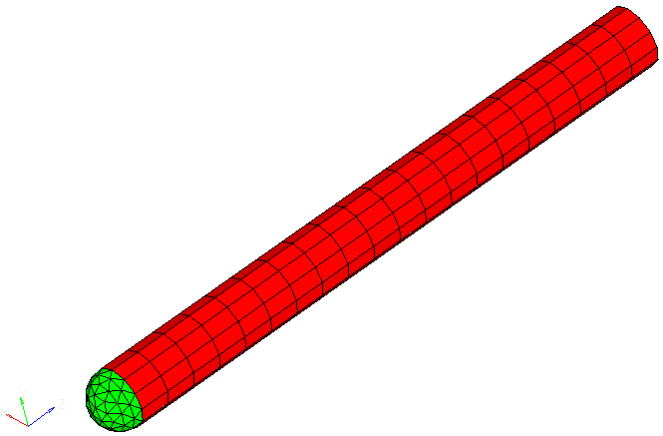

Fig. 3.4.1: Outer hull structure

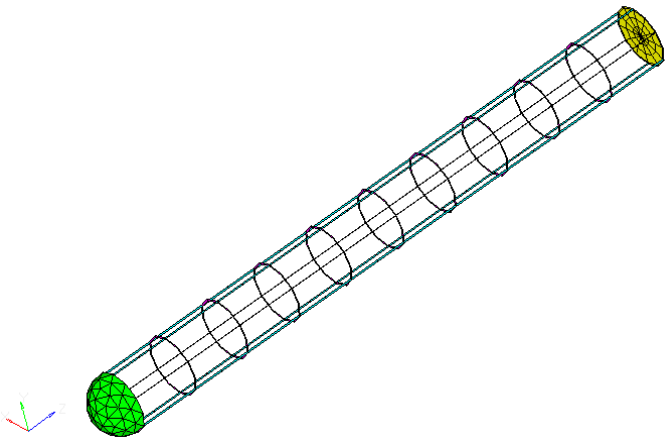

Fig. 3.4.2: Inner hull structure

The model was saved as a text file in standard NASTRAN format. The NASTRAN-format text file was then run through a Pre-EFEA program which accompanies the EFEA program. The pre-processing program converted the NASTRAN-format file into another text file with the data formatted so that it is readable by the EFEA program. Additionally, the user must edit this text file to include the loading conditions and indicate the desired output. A simple MATLAB function was developed to automatically edit this text file to vary the plate thicknesses (design variables) as design points were evaluated during the optimization.

The EFEA program was called directly from MATLAB. After the program analyzed a design, it output a text file containing the amplitude of the velocity of vibration at each node in the finite element model. To summarize this data into a single scalar value, the average over the entire vehicle was taken. Other possible ways to condense the data into a single value were considered, including weighted averages or studying only data at "important" areas of the vehicle where scientific instruments would be attached. However, the average approach seemed most appropriate without information on the placement of any scientific instruments because it includes data from the entire vehicle which could help ensure that the effects of all of the design variables are included in the objective.

To summarize the procedure used to evaluate the objective function:

Step 1: Create a finite element model of the hull

Step 2: Use the pre-EFEA analysis tool on the finite element model

Step 3: Modify the input file to include loading conditions and indicate desired output

Step 4: Run the EFEA program at the desired design point

Step 5: Postprocess the results to determine the average vibration response

Constraints

The constraints for the design consist of one constraint on the total mass of the hull structure and four constraints on the stresses in the structure.

The constraint on the total mass of the hull structure, M_{TOT} (measured in kg). This constraint is important for two reasons: first, it is important that the weight of the structure does not dominate the vehicle because the vehicle must also be able to carry batteries, instruments, and other equipment; and second, it is expected that in general, increasing the hull structural member thicknesses will result in reduced vibrations (improved objective function performance), so the limit on the total mass will help keep the optimization problem bounded.

The total mass can be computed (based simply on the geometry) as

$$M_{TOT} = \rho_h \left(t_h \pi D L + 6 L h_l t_l + \pi \left(\frac{D}{2} \right)^2 t_e + 2\pi \left(\frac{D}{2} \right)^2 t_n + 10 \pi t_r \left[\left(\frac{D}{2} \right)^2 - \left(\frac{D - h_r}{2} \right)^2 \right] \right) \qquad (3)$$

The diameter and length of the vehicle are treated as parameters for the vibrations analysis, but the diameter and length are design variables for other subsystems. Because the total mass of the structure depends on these parameters (which will eventually be modified in the multi-subsystem optimization), the maximum total structural mass is determined as a percentage of the buoyancy, rather than as a fixed value. Therefore, the constraint on the total mass becomes

$$100 \frac{M_{TOT}}{M_{BUOY}} \leq 50 \qquad (4)$$

where 50 indicates that the maximum allowable ratio of structural mass to buoyancy is 50% (hence the multiplication by 100 on the ratio on the left side). The choice to formulate the constraint in this manner is also an issue of scaling, which is discussed further in the Model Analysis section of the report. M_{BUOY} is the mass of water displaced by the hull, which is given by

$$M_{BUOY} = \rho_w \left[\pi \left(\frac{D}{2} \right)^2 L + \frac{2}{3} \pi \left(\frac{D}{2} \right)^3 \right] \qquad (5)$$

The decision to limit the mass of the hull to 50% of the displaced mass is somewhat arbitrary. The value of 50% is reasonable, because it allows half of the mass of the vehicle to be comprised of the other subsystems (propulsion and maneuvering equipment) and the scientific instruments that the vehicle is designed to carry. However, because this value was chosen arbitrarily, a parametric study showing the effects of the maximum allowable mass ratio is included in the Parametric Study section of the report.

The next four constraints concern the stresses in the hull. The vehicle will be operating deep underwater which leads to high pressures on the hull, so it is important to ensure that the hull structure will be adequate.

The simplest stress to evaluate is the stress in the circular end plate. To simplify this model, effects of the attachment of the propeller are neglected and the end of the hull is modeled as a simple flat, circular disk with fixed edges. Then the maximum stress can be computed according to (Boresi, Schmidt 2003)

$$\sigma_e = \frac{3}{4} p \left(\frac{D}{2t_e} \right)^2 \qquad (6)$$

where p is the pressure on the hull.

The stresses in the hemispherical nose of the vehicle can be approximated according to (Hearn 1985)

$$\sigma_n = \frac{pD}{4t_n} \qquad (7)$$

The stresses in the stiffeners are analyzed using a simple beam bending approximation. The hull is divided into strips along each stiffening member and the strip is treated as a beam under a bending load (water pressure). This calculation requires several intermediate steps with the details included in Appendix B. The calculation concludes in the evaluation of the stresses

$$\sigma_r = \frac{M_r c_r}{I_r} \qquad \text{in the rings} \qquad (8)$$

$$\sigma_l = \frac{M_l c_l}{I_l} \qquad \text{in the longitudinal stiffeners} \qquad (9)$$

where M_r and M_l are the maximum bending moments, c_r and c_l are the maximum distances from the neutral axis, and I_r and I_l are the moments of inertia.

Finally, the constraints on the stresses can be expressed:

$$\sigma_e \le \sigma_{\max} \qquad (10)$$

$$\sigma_r \le \sigma_{\max} \qquad (11)$$

$$\sigma_l \le \sigma_{\max} \qquad (12)$$

$$\sigma_n \leq \sigma_{\max} \qquad (13)$$

Design Variable Bounds

Practical lower and upper bounds were included on the design variables. Although it may be physically possible to describe the thicknesses by $t_i > 0$, this is not a practical constraint for several reasons. First, it is not possible to include the open constraint in the optimization algorithm; the algorithm takes only bounds of the form $x_L \leq x \leq x_U$ (not $x_L < x < x_U$). Second, it is not expected that any physically reasonable designs would be encountered with thicknesses very close to zero; extremely thin plates would be difficult to manufacture and would likely be impractical when considering welding, propeller attachment, and other factors not described by this model. Therefore, a lower bound of 1 mm was initially selected for all of the thicknesses. However, numerical difficulties were encountered with the lower bound on the hull thickness t_h of 1 mm and the optimization was unable to determine a minimum, so the lower bound was increased until the optimization ran successfully, giving the lower bound on the hull thickness of 4 mm.

An upper bound for the thicknesses was also included. A thickness of more than 10 mm (1 cm) quickly becomes too heavy; in fact, if the outer hull thickness is 10 mm, the mass of the hull alone is greater than 50% of the displaced mass. Therefore, the maximum thickness of 10 mm constitutes a reasonable upper limit on the plate thicknesses.

3.4.2 Vibrations Model Analysis

Monotonicity Analysis

Monotonicity analysis can be applied to an optimization problem to determine if the problem is well-bounded. The problem is well bounded if at least one constraint has opposite monotonicity of the objective function.

Because the objective function is a simulation, instead of an analytical expression, it is not possible to directly determine the monotonicity of the objective function. However, if it can be shown that there are constraints of both positive and negative monotonicity for each design variable, it is safe to conclude that the function will be well-bounded because it can be bounded

by either the positively monotonic constraint or the negatively monotonic constraint (in each design variable).

First, the constraint on the mass ratio, constraint g_1 in Equation (14), can be analyzed. The displaced mass, M_{BUOY}, is a constant. However, it can easily be seen in Equation (3) that the total hull structure mass increases linearly with each design variable (t_e, t_h, t_l, t_n, t_r).

The constraint g_2 in Equation (14) corresponds to the stress computed in Equation (6), which clearly decreases with increasing t_e; the other design variables do not appear in constraint g_2. The constraint g_3 corresponds to the stress computed in Equation (7), which decreases with increasing t_n; the other design variables do not appear in constraint g_3.

For the remaining constraints g_4 and g_5, the monotonicity properties are not immediately clear. For both stresses σ_r and σ_l, the numerator includes the distance c which depends on the design variables in a complex manner, and the denominator includes the moment of inertia I, which also depends on the design variables. Therefore, rather than take an analytical approach to determine the monotonicity of g_4 and g_5, a numerical/graphical approach is used.

Each of the two constraints g_4 and g_5 depends on only two of the design variables: g_4 depends on t_l and t_h, and g_5 depends on t_r and t_h. The stresses σ_r and σ_l can be plotted as functions of their respective design variables over their allowable ranges and information about the behavior of the constraints can be determined from the plots. Figure 3a shows the three-dimensional plot of the stress σ_l as a function of t_l and t_h, and Figure 3b shows the two-dimensional contour plot corresponding to Figure 3a. Figure 4a shows the three-dimensional plot of the stress σ_r as a function of t_r and t_h, and Figure 4b shows the two-dimensional contour plot corresponding to Figure 4a.

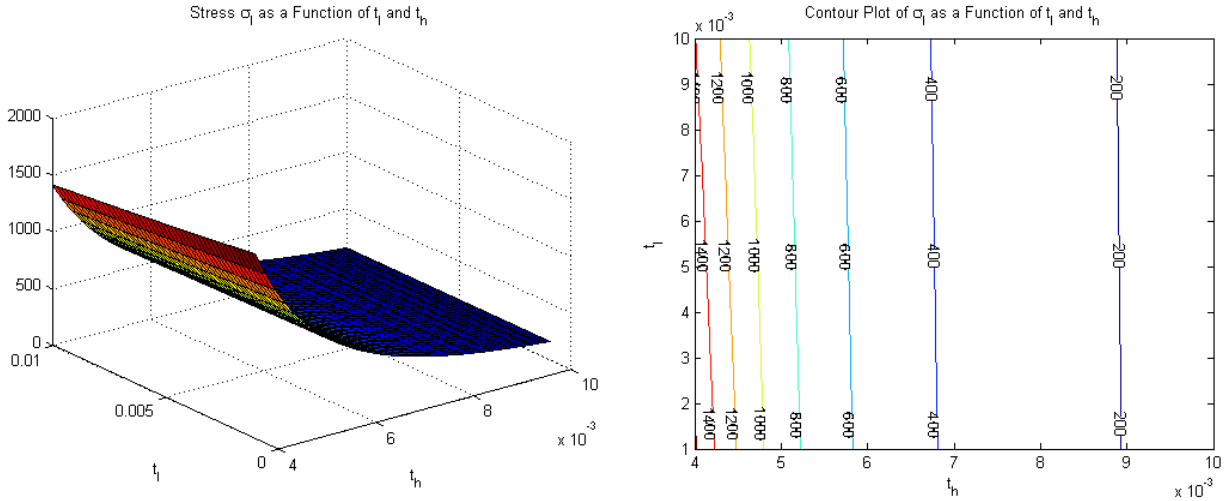

(a) (b)

Fig. 3.4.3: (a) Surface plot of the stress σ_l as a function of t_h and t_l. (b) Contour plot corresponding to 3.3.3(a).

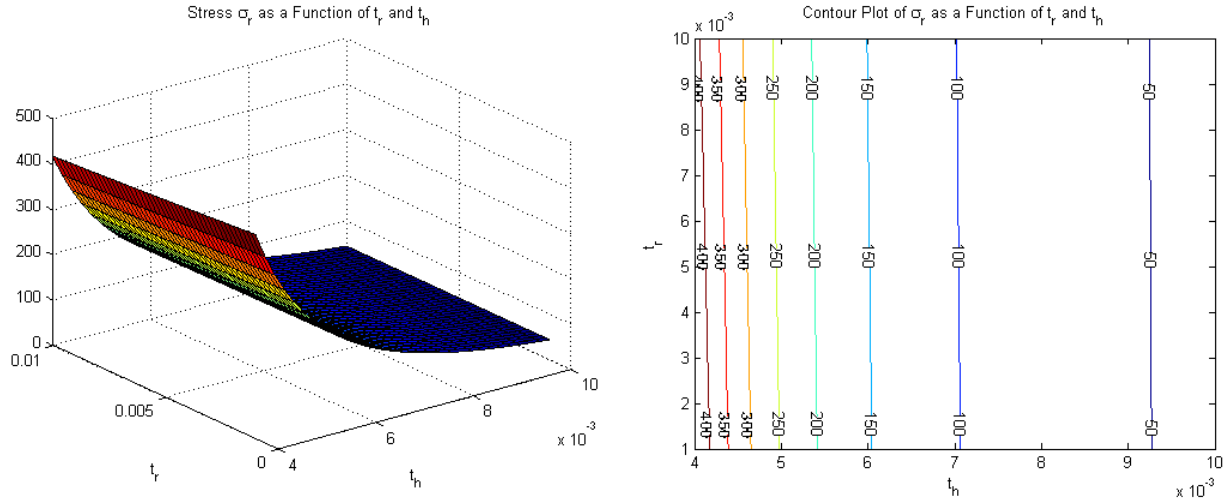

(a) (b)

Fig. 3.4.4: (a) Surface plot of the stress σ_r as a function of t_h and t_r. (b) Contour plot corresponding to 3.4.4(a).

Both Fig. 3.4.3a and Fig. 3.4.4a show a surfaces for the stress that increase as the thicknesses decrease. To verify that this is indeed the response, a contour plot is provided in Fig. 3.4.3b and Fig. 3.4.4b which shows only increasing behavior as the thicknesses decrease. Therefore, we can safely conclude that constraint g_4 decreases with t_l, and t_h and g_5 decreases with t_r and t_h.

The results of the monotonicity analysis are summarized in Table 3.4.1. The "+" symbol indicates that the constraint increases in the specified design variable, while "–" indicates that the constraint decreases in the specified design variable.

Table 3.4.1: Monotonicity analysis summary					
	t_e	t_h	t_l	t_n	t_r
g_1	+	+	+	+	+
g_2	−				
g_3				−	
g_4		−	−		
g_5		−			−

Table 3.4.1 illustrates an important property of the constraints for this optimization problem: for each design variable, there is a constraint which increases in that variable, and another constraint which decreases in that design variable. This allows for the critical conclusion that the monotonicity properties of the objective function are not necessary in order to conclude that this problem is well-bounded. If the objective function is increasing or decreasing in any variable, there will be (at least) one constraint with opposite monotonicity in that variable to bound the objective function.

Constraint Redundancy and Activity

As shown in the monotonicity analysis, the constraint on the mass ratio (constraint g_1) has opposite monotonicity of the other constraints; therefore, it is not expected that constraint g_1 will be redundant with any of the other constraints. Constraints g_2 and g_3 depend only on t_e and t_n, respectively, and these design variables do not appear in the remaining constraints g_4 and g_5, so there is no redundancy in the constraints g_2 and g_3. Constraints g_4 and g_5 both depend on the design variable t_h, however, g_4 also depends on t_l while g_5 depends on t_r. Therefore, redundancy is generally not expected in the constraints g_4 and g_5 because they depend on different variables.

Constraint activity cannot be determined without any specific analytical information about the monotonicity behavior of the objective function. However, it is expected that, in general, increasing the plate thicknesses will result in reduced vibrations (improved objective function response). Therefore, the mass ratio constraint (g_1) will likely be active at the optimum.

Scaling

To improve the performance of the optimization algorithm, the constraints were scaled to a similar magnitude in their numerical implementation. Recall that the constraint on the mass ratio,

g_1, was scaled by 100 so that instead of a percentage value in the range [0, 1], the mass ratio would have a value in the range [0, 100]. In coding the stress constraints, g_2 through g_5, the stresses were scaled by a factor of 10^{-6} so that the stresses would be in units of MPa, instead of Pa. Recall that the maximum allowable stress is 200 MPa; with this scaling all of the constraints should be comparing values of order 10^2.

3.4.3 Vibrations Results and Parametric Study

The optimization was initially attempted using MATLAB's fmincon function. However, the algorithm was unable to reach any feasible point other than the (feasible) starting point. The gradient-based algorithm may have encountered difficulties computing the gradient with the simulation-type objective function. Therefore, the non-gradient-based DIRECT algorithm was used for this optimization. The DIRECT algorithm did not require input of a starting point for the optimization, and it was able to locate feasible points; however, the DIRECT algorithm was significantly slower than fmincon. One run of the optimization using DIRECT took approximately 20 minutes, depending on how quickly the algorithm converged.

Because the DIRECT algorithm did not require the input of an initial starting point, the global convergence properties of the optimization cannot be investigated by varying the starting point. However, DIRECT is considered a global search algorithm so it is assumed that the optimum points returned using DIRECT are global optima.

The optimization yielded a minimum vibration of 0.0280 m/s, with the values of the design variables at the optimum given in Table 3.4.2. At the minimum, the value of the mass ratio was 49.7%, indicating that the constraint on the mass ratio was active; this agrees with the expectations from the monotonicity analysis. The constraint g_2 on the stress in the end of the vehicle was also active. The variable bounds on the design variables t_e, t_h, t_l, and t_n were not active at the minimum; the value of t_e at the minimum was 9.83 mm, which is close to the upper bound of 10 mm, but not active. Therefore, it is safe to conclude that the variable bounds, which were somewhat arbitrary, did not artificially bound the problem.

Table 3.4.2: Optimum design variable values	
Design Variable	Value at Minimum (mm)
t_e	9.8333
t_h	8.9259
t_l	2.3148
t_n	1.3148
t_r	3.9444

In the project proposal, a feasible point was located to show that the design space was not empty. That feasible point was (t_e, t_h, t_l, t_n, t_r) = (0.0065, 0.009, 0.003, 0.002, 0.003) m. At this point, the value of the objective function was 0.0407 m/s, which shows the significant improvement achieved at the minimum of 0.0280 m/s.

Parametric Study

The geometric properties of the hull such as length, diameter, and stiffener height were defined within the finite element model. Modification of these parameters must be done by hand (within Hypermesh), and requires that the model be re-exported and re-preprocessed. Therefore, parametric studies of the geometric factors were not considered because of the time-consuming manual nature of the modifications.

The monotonicity analysis indicated that the mass ratio constraint would be active, and the results of the optimization confirmed this. Therefore, it is important to consider the effects of the somewhat arbitrary maximum value of 50%. The optimization was re-run with varying values of the maximum allowable mass ratio and the results are plotted in Figure 3.4.4. Figure 3.4.4 shows that as the maximum allowable mass ratio is increased, the minimum velocity of vibration decreases, but after about 55% the constraint becomes inactive and has no effect on the optimum. This occurs because at a mass ratio of about 55% and higher, the mass ratio constraint becomes redundant with the design variable upper bounds. A mass ratio higher than approximately 55% cannot be obtained without increasing the plate thicknesses beyond 10 mm.

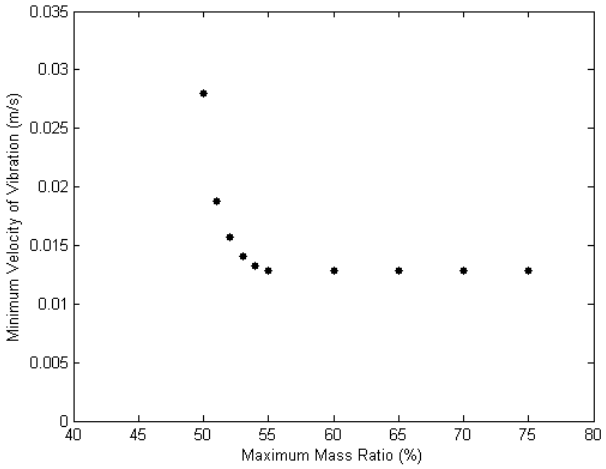

Figure 3.4.4: Results of parametric study showing the effect of the maximum mass ratio.

Although the variable bounds were not active in the solution of the original optimization problem, the above parametric study illustrates the potential importance of the somewhat arbitrary upper bound. The optimization was run again with the upper bound increased to 11 mm for all of the thicknesses. The resulting values of the design variables are given in Table 3.4.3, with the minimum vibration velocity of 0.0369 m/s. The upper bound on the design variables (11 mm) is not active at this minimum, but the constraint on the mass ratio is active. It is interesting to note that although the design space was expanded by increasing the possible values for the design variables, the solver did not reach the same minimum achieved in the original optimization. One possible explanation for this phenomenon is that the search method used by DIRECT divides the design space into different subspaces (rectangles); changing the bounds on the design variables changed the way the design space was divided, yielding a different search pattern and ultimately a different optimum.

Table 3.4.3: Design variable values from parametric study

Design Variable	Value at Minimum (mm)
t_e	6.8642
t_h	8.9403
t_l	2.0905
t_n	1.3086
t_r	7.9753

3.4.4 Vibrations System Level Tradeoffs

When the vibrations subsystem is combined with the other subsystems for the overall vehicle design, the subsystems will affect each other. The length and diameter of the vehicle are used by all four subsystems (maneuvering, propulsion, controls, and vibrations) and these dimensions are important in determining the response of the vehicle in all of the subsystems. Therefore, it is important to consider the potential effects of varying the length and diameter on optimization problem for vibrations analysis. One effect that was considered in the formulation of the vibrations problem is the constraint on the maximum mass of the vehicle. Rather than fixing a value for the maximum structural mass, the constraint was written as a percentage of the displaced mass of the vehicle to better facilitate changes in the dimensions.

Although the constraint on the maximum mass of the structure was written in a dimensionless form, the bounds on the thicknesses were not. It is expected that as the vehicle becomes larger, greater thicknesses will be required to meet the requirements for the stresses. Therefore, the bounds on the thicknesses may be adjusted in the system optimization.

It is expected that the vibrations subsystem will have the most interaction with the maneuvering subsystem. The weight distribution of the vehicle is an important factor in determining the maneuvering behavior, and the weight distribution is directly affected by the thicknesses of the structural members.

4. System Integration Study

In the individual subsystem analyses, the effects of linking the four subsystems into one system problem were considered. The goal of the system integration study was to resolve these issues and create an overall system problem.

The maneuvering subsystem design will be significantly influenced by the other subsystems. Forward speed was shown to effect turning radius in a parametric study. In the system level design, the forward speed will be subject to the thrust provided by the propeller. The efficient operating range for the propeller may be above the low speeds shown to yield smallest turning

radius. The structures subsystem will influence the maneuvering characteristics of the vehicle through the mass, since a heavier vehicle corresponds to a larger turning radius.

When the global objective function includes the effects of control effort and state excursion, the control optimization will indirectly influence the choice of the system design variables. The most significant impact is due to the vehicle speed; a greater forward speed correlates to greater control surface forces, which give improved performance.

Optimization of the vehicle for the maximum propeller efficiency requires more than reducing the drag by reducing vehicle size. Increased control force induces more drag into the system and therefore reduces the overall efficiency. The vehicle speed is important for the maneuvering discipline because increasing speed increases the turning radius. In addition, increasing the vehicle speed also decreases the propeller efficiency.

For the vibration subsystem, the constraint on the maximum mass of the vehicle is important for the system integration. Rather than fixing a value for the maximum structural mass, the constraint was written as a percentage of the displaced mass of the vehicle to better facilitate changes in the dimensions, since the length and diameter were updated for the system problem. The vibrations subsystem will have the most interaction with the maneuvering subsystem because the weight of the vehicle is an important factor in determining the maneuvering behavior.

For the system integration study, the subsystem model information must be combined to form an overall system model. However, this system problem must have only a single objective function, because multi-objective optimization is not within the scope of this project. Therefore, the first step in defining the system problem was to determine a system level objective function. The system objective function was selected to be the maximization of the vehicle speed (U). The vehicle speed was selected to be the system objective because a faster vehicle can cover more area in less time, making an underwater survey of a specific area more time efficient.

Maximization of the vehicle speed also presents an excellent overlap between the four subsystems. The vehicle speed has a clear impact on the maneuvering performance; increasing the speed increases the turning radius of the vehicle. The vehicle speed affects the controls subsystem because increased speed gives a larger control force on the fins, leading to reduced control effort. The propulsion subsystem is affected by the vehicle speed because the propeller efficiency is directly impacted by the speed. The vehicle speed is indirectly related to the structural design through the weight of the hull which is an important factor for the maneuvering.

Therefore, the system level problem used maximization of the vehicle speed as the objective, and each of the subsystem level objectives were converted into constraints. The average amplitude of the hull vibrations must be less than 0.06 m/s. The propeller efficiency must be greater than 40%. The turning radius must be less than 30 m for a constant rudder angle of 5°. The controls squared error must be less than 500 m^2s (squared path error integrated over the trajectory) and the control effort must be less than 200. Additionally, the original constraints for each of the subsystems were included. The diagram in Figure 4.1 summarizes the AIO (all-in-one) system problem.

In the individual optimizations, the controls, propulsion, and structural design subsystems treated the length and diameter of the vehicle as parameters. However, the maneuvering subsystem used the length and diameter as design variables to determine the optimum geometry for maneuvering. For the system optimization problem, the length and diameter were set as parameters using the values determined from the maneuvering subsystem analysis. The length and diameter could not be treated as design variables in the system problem because the geometry could not be directly altered for the structural finite element model.

The mass ratio constraint for the structures was changed to the hull mass as a percentage of the vehicle mass (M) instead of as a percentage of the displaced mass. This improved integration between subsystems, and the maximum percentage was increased to 80%.

In the overall system optimization the number of blades was held constant to help the DIRECT algorithm converge. Furthermore, the difference in efficiency between a two-bladed and a three-

bladed propeller is minimal, but two-bladed propellers are easier to manufacture and therefore more affordable.

Since the relation of propeller diameter and efficiency showed strong monotonic behavior, the propeller diameter was held fixed at the maximum value. The upper bound is defined for hydrodynamic reasons, as discussed above.

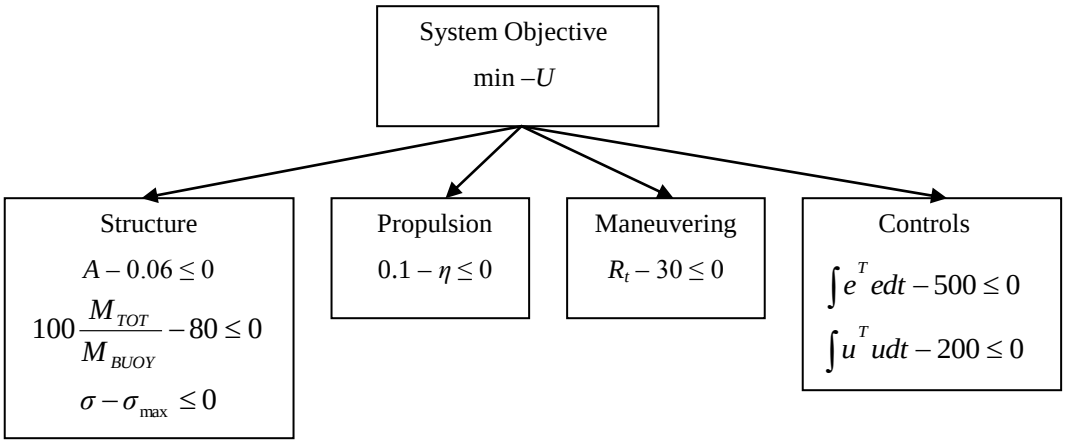

Fig.4.1: Summary of the system optimization problem.

Design variable bounds were chosen based on successful results from subsystem optimizations and are summarized in Table 4.1.

Table 4.1: Design variable bounds

Design Variables	Lower Bound	Upper Bound
t_e	1	10
t_h	1	10
t_r	4	10
t_l	1	10
t_n	1	10
k_1	0	2
k_2	0	0.2
k_3	0	10
k_4	0	0.2
k_5	0	10
k_6	0	0.2
M	20	40
U	1	50
N_b	2	2
A_E/A_0	0.4	1.05
D_p	0.15	0.15

The system optimization problem was solved using the DIRECT algorithm implemented in MATLAB. The algorithm was set to run for 7000 function evaluations, which took about 13 hours to run. The results of the optimization are summarized in Table 4.2.

Table 4.2: Summary of optimizers for system optimization and individual subsystems

Design Variables	AIO Optimal	Maneuvering	Controls	Propulsion	Vibrations
t_e	2.500				6.864
t_h	5.500				8.940
t_r	7.000				2.091
t_l	5.500				1.309
t_n	5.500				7.975
k_1	1.667		0.192		
k_2	0.100		0.000		
k_3	1.000		1.060		
k_4	0.033		0.640		
k_5	5.000		6.289		
k_6	0.100		0.0047		
M	30.000	12.9			
U	2.500	1.0			
N_b	2.000			3.000	
A_E/A_0	0.942			0.400	
D_p	0.150			0.152	

The results in Table 4.2 illustrate one of the problems encountered with using DIRECT. The DIRECT algorithm works by successively splitting the design space into rectangular areas. However, with such a large number of design variables (16), the algorithm requires an extremely large number of evaluations to resolve the design space into different regions. Because of time constraints, the program could not be run for more than several thousand iterations, and in this time the algorithm may not have been fully able to explore the design space. This explains why several of the design variables settled at values near one-half, one-quarter, etc. of their range.

The resulting system optimum design gave a maximum vehicle speed of 2.5 m/s.

The global optimization yielded a much larger turning radius than the subsystem optimization. This could be expected as turning radius was a constraint in the global optimization while it was the objective to be minimized in the subsystem design. In the global problem, it was thought that

the vibration constraint would bound the mass variable from the bottom while the turning radius constraint would provide an upper bound. For the vibration of the vessel to remain below a maximum constrained value, the stiffeners must have some minimum strength. As the stiffeners become stronger they will become heavier. On the other hand, a heavier vessel turns slower, therefore if the stiffeners became too heavy the turning radius constraint would be violated. The global optimization results, however, indicated that overlarge stiffeners were not an issue. The optimum turning radius from the subsystem analysis is 5.9 meters at a 5^o rudder angle. The global value was 17.1 meters. The constraint was set much higher than the subsystem optimum because high speeds were expected. Turning radius increases dramatically with speed. Even so, a 17.1 meter turning radius for a 1.5 meter vessel at such a slight rudder angle seems to be an acceptable result. The rudder angle was set so low in hopes of limiting the rudder effects. Obviously, rudder angle is required to turn the AUV, however the low-fidelity rudder model fails to capture turbulent effects accurately.

Mass was a variable used in both the subsystem and global optimizations. Mass was represented as an overall density for the subsystem optimization. This linked the size of the vehicle with its weight, thus modeling the likely relationship of mass and vehicle size. The weight range used to bound mass for the subsystem was very low, on the order of 6 lbs (2.7 kg). This is an extreme case used to highlight the minimum possible turning radius. For the group optimization, a more realistic bound was set at 40 kg. The optimum mass was 30 kg, which yielded a turning radius well below the constraint and a vibration amplitude well below the constraint. This value rendered both the structures and maneuvering disciplines inactive. Unfortunately, the DIRECT program requires a feasible point to be located at the center of the variable bounds and despite 7,000 iterations, the program never bounced against the bounds.

In the global optimization both control effort and squared error along the trajectory are treated as constraints. The bounds for these constraints were determined by examining objective values for reasonable trajectory outputs from the controls subsystem optimization. The AIO optimal control gain vector is in relatively good agreement with the values obtained in the subsystem analysis. Neither constraint was active during the optimization, which follows logically from the

knowledge that both control effort and squared error should be reduced at higher forward speeds due to larger control forces.

The behavior of the propulsion system was evaluated at the system optimum; the results are summarized in Table 4.2. The overall system optimum reduced the propeller efficiency by 3.2% to $\eta_0 = 48.7\%$.

Table 4.2: Propulsion summary at system optimum

Variable	Value
A_E/A_0	0.9417
N_b	2
D_P	0.15 m
P/D_P	1.4
U	1318.4 rpm
V_k	2.5 m/s
η_0	48.7 %

Since the speed was more than doubled for the overall system optimization the propeller had to be adapted to the new operating speed.

A_E/A_0 has been increased to a very high value to reduce the pressure gradient along the propeller blade. Since the propeller is producing about 6.25 times more thrust to achieve the higher velocity, it is very likely to cavitate. Increasing the propeller blade area raises the water pressure behind the propeller and therefore prevents the occurrence of cavitation. Additionally, a high propeller blade area allows for more pitch, which increases the efficiency.

A high pitch is always favorable since it increases the efficiency of the propeller tremendously, but usually a lower-than-theoretically ideal pitch must be chosen to reduce the effects of cavitation. Since a very high expanded area ratio was chosen by the optimizer the pitch could reach its maximum. This indicates a tradeoff between the two parameters, showing that a higher pitch compensated by a high A_E/A_0 is more favorable than a low propeller blade area compensated by a lower pitch.

To produce enough thrust the propeller speed had to be increased by a factor of 2.3. The resulting 1318.4 rpm is a high value, which would easily lead to cavitation if the geometry had

not been changed, as discussed earlier. Nevertheless a lower rpm would be more favorable, but would lead to too much torque load for the motor.

An overall loss of efficiency of only 3.2% is a very small value compared to the thrust that was increased by 625%. Since a propeller is best described as a rotating airfoil, certain similarities occur. As an airfoil, a propeller has an optimal operating point and it is reasonable to assume that the flow velocity around the propeller in the individual optimization was too slow to reach the best ratio of drag and lift. This explains why the speed during the subsystem optimization did not converge against its lower bound.

The new velocity seems to suit the propeller's geometry characteristics better than the lower speed of the vehicle during the individual subsystem optimization, resulting in a better ratio of lift and drag.

For the individual subsystem optimization, the optimal structural design yielded a minimum average vibration velocity of 0.0280 m/s. Also, in the individual problem, the mass ratio constraint was limited to 50% of the displaced mass, and this constraint was active at the minimum with a value of 49.7%. For the system optimization problem, the optimal structural design yielded a minimum average vibration velocity of 0.0526 m/s; this is significantly larger than the minimum encountered for the individual problem. However, it is difficult to compare these results because the geometry (length and diameter) of the vehicle was altered from the original subsystem analysis to the AIO optimization. Also, at the global optimum, the value of the mass ratio was 51.6%; the maximum allowable value was 80% indicating that the constraint was not active. Although in the individual analysis it was anticipated that the mass ratio constraint would be active (and it was), it is not surprising that the constraint is no longer active in the system optimization because of the interactions with the maneuvering analysis.

Through this study, we have presented an optimization framework for a general purpose AUV. The results demonstrate global level tradeoffs between vehicle subsystems yielding an overall system optimum.

References

Boresi, A. P., Schmidt, R.J. *Advanced Mechanics of Materials*. 6e. John Wiley and Sons, 2003.

Fossen, T. *Guidance and Control of Ocean Vehicles*. Wiley and Sons, New York, NY, 1999

Hart, C.G., Vlahopoulos, N., *A Multidisciplinary Design Optimization Approach to Relating Affordability and Performance in a Conceptual Submarine Design,* University of Michigan, 2009.

He, J., Zhang, G., Vlahopoulos, N. (2009) Vehicle airborne noise analysis using boundary element and finite element energy based methods. SAE Paper 2009-01-2222.

Hearn, E. *Mechanics of Materials*. Butterworth-Heinemann, 1985.

Leveille, E. *Analysis, Redesign and verification of the Iver2 Autonomous Underwater Vehicle Motion Controller*. M.S. Thesis, 2007.

de Lima, W.J., Vlahopoulos, N., Sbragio, R., He, J. (2009) Interior aircraft noise computations due to TBL excitation using the energy finite element analysis. SAE Paper 2009-01-2248.

Ogata, K. *Discrete-Time Control Systems*. Prentice Hall, Inc, Upper Saddle River, NJ, 1995

Prestero, T. *Verification of a Six-Degree of Freedom Simulation Model for the REMUS Autonomous Underwater Vehicle.* M.S. Thesis, 2001.

Stengel, R. *Optimal Control and Estimation*. Dover Publications, Mineola, NY

Vlahopoulos, N., Wu, K. (2010) Simulation technology for noise and vibration design of naval vehicles. American Society of Naval Engineers ASNE Day 2010 Conference, Arlington, VA.

Zhang, G., Wang, A., Vlahopoulos, N. (2009) Engaging energy based structural-acoustic simulations in multi-discipline design. SAE Paper 2009-01-2198.